Open Access

Recent Progress in Materials

LIDSEN Publishing Inc.

Research Article

Calculation of the Forces Applied to a Superconductor in Levitation in an Inhomogeneous Magnetic Field

Pierre Bernstein *, Yiteng Xing, Jacques Noudem

CRISMAT-CNRS, ENSICAEN, Normandy University, Caen, France; E-Mails: pierre.bernstein@ensicaen.fr; Yiteng.Xing@ensicaen.fr; jacques.noudem@ensicaen.fr

* **Correspondence:** Pierre Bernstein; E-Mail: pierre.bernstein@ensicaen.fr

Academic Editor: Michal Nowicki

Special Issue: New Trends in Magnetic Materials

Recent Progress in Materials
2022, volume 4, issue 3
doi:10.21926/rpm.2203018

Received: July 07, 2022
Accepted: August 30, 2022
Published: September 15, 2022

Abstract

Stable levitation of systems consisting of a magnetic source and a superconductor is actively investigated due to the promising applications of this technology. While huge efforts have been made for modeling these setups with numerical simulations, analytical models, in spite of their use being limited to devices with a high degree of symmetry, can bring precious information on certain characteristics of levitating systems. Summarizing our previous work in the field, we present the mean-field model that we have proposed to reproduce the interactions between a magnetic source and a superconductor. We show that the model provides an estimation of the surface critical current density of the shielding currents flowing in the superconductor and an estimation of the thickness, *t*, of the layer carrying the currents. We emphasize that the calculated values of *t* are an increasing function of temperature, which tend toward the Meissner limit at low temperatures. Finally, we determine the condition that ensures stable levitation of axisymmetric systems.

Keywords

Magnetic superconducting levitation; mean field model; stability condition

1. Introduction

Superconducting magnetic levitation (SML) involves the stable levitation of superconductor(s) above a source of magnetic field. The most promising applications of this technology are the auto-stabilized high-velocity rotating magnetic bearings with no mechanical contacts [1-4] on the one hand, and magnetic levitating (MAGLEV) trains on the other hand [5-10]. The first MAGLEV train has been running on a demonstration track at the Federal University of Rio de Janeiro in 2014 [11] (see Figure 1). Recently, a MAGLEV train prototype designed for running at 620 km/h was demonstrated in China [12].

Figure 1 SML MAGLEV prototype on the demonstration track built at the Federal University of Rio de Janeiro.

The force of interaction between a levitating superconductor and the system generating the magnetic field consists of the levitation force and the guidance or lateral force that secures the stability of levitation. The lateral and levitation forces depend on the distance, Z_{cp}, between the field source and the superconductor when the superconductor is cooled down in opposite ways: the larger the value of Z_{cp}, the larger is the levitation force and the lower is the restoring force [13]. In some cases, there is a threshold for Z_{cp} above which levitation is unstable [14]. To date, different numerical and analytical approaches have been proposed for determining these forces. As in the case of any electromagnetic setup, numerical simulations generally employ finite elements methods (FEMs) for solving Maxwell's differential equations. Superconductivity is accounted for by introducing a so-called power law between the electric field, E, and the current density, J. This law generally takes the form

$$E = E_c \left(\frac{J}{J_c}\right)^n \tag{1}$$

where E_c is usually the electric field criterion employed for defining the superconductor critical current density, J_c, whereas the exponent n is proportional to the activation energy of vortex

depinning. FEMs allows determining $\vec{J}$ as well as the field, $\vec{B}$, generated by the magnetic source everywhere in the superconductor. The force of interaction with the magnetic system is written as

$$\vec{F} = \int_{\mathcal{V}} \vec{J} \times \vec{B} d\mathcal{V} \quad (2)$$

where $\mathcal{V}$ is the superconductor volume. The capability of the FEMs to mesh complex shapes has been exploited to simulate realistic SML systems (see [15-19] as examples). In contrast, analytical models generally require a regular distribution of the applied field and are practical in their use for simple superconductor shapes with a high level of symmetry only. However, they have the advantage of representing physical laws that are not always obvious from the results of simulations. The best-known analytical technique is the magnetic image model. When a superconductor is cooled down below the temperature of transition to the superconductor state, T_c, the magnetic moment of the magnetic source generates a "frozen" symmetrical image moment with respect to the superconductor surface [20]. The normal component of the field created at the surface of the superconductor by the frozen moment is equal to that generated by the magnetic source moment. The total field at the surface of the superconductor must not change with the location or orientation of the magnet, which allows determining the image moment at any position and the resulting forces. An advantage of the magnetic images model is that, with suitable changes, it can account for lateral displacements as well as vertical ones [21]. It allows the calculation of the forces and torques between the superconductor and the magnetic source, even if their surfaces are not parallel. Hence, considering the use of the magnet-superconductor interactions for the docking of two spacecrafts, some researchers have modeled the process with this technique [22, 23]. However, for obtaining accurate results, the magnetic source should be modeled not as a single magnetic dipole but as a set of magnetic dipoles [24], which complicates the calculations.

In this article, we describe a simple mean field analytical model used for calculating the lateral and levitation forces of SML systems and determining their stability condition. Section 2 describes the procedures that have been used for measuring the levitation and lateral forces. The mean field model and its application to the reproduction of the forces of interaction between the magnet and the superconductor have been described in Section 3. The end of Section 3 is dedicated to a discussion on the advantages and limitations of the model. Section 4 summarizes the most important results obtained from this work.

2. Measurements

In this section, we describe the procedure used for measuring the levitation and the lateral forces of the levitating system. For the sake of clarity, we describe the simplest system, which consists of a bulk superconductor and a permanent magnet. Examples of the systems used in our laboratory for measuring these forces are shown in Figure 2. For measurements at 77 K, the sample was kept in an open cryostat filled with liquid nitrogen (left side of Figure 2), whereas for measurements below 77 K, the superconductor was kept in a cryostat cooled down by a cryo-cooler (right side of Figure 2). The measuring system included a 3-axes positioning system as well as vertical and lateral force sensors. To carry out the measurements, firstly, the magnet was fixed to the positioning system at a distance of Z_{cp} from the superconductor. Then, the superconductor was cooled down below its transition temperature. For measuring the levitation force, after temperature

stabilization, the mobile magnet was moved vertically from Z_{cp} *to* Z_{min}, the smallest possible separation between the magnet and the superconductor. At Z_{min}, the motion of the magnet was reversed, and the magnet was driven up to Z_{cp} or above (see Figure 3). The levitation force was measured at each step of the process. For measuring the lateral force (see Figure 4), after temperature stabilization at Z_{cp}, the magnet was driven to a distance of Z from the superconductor. Then, it was moved parallel to the superconductor surface to Y_1, where the direction of motion was reversed, and the distance Y decreased to Y_2 before increasing to $Y = 0$. The lateral force was recorded as a function of Y. The distances Z and Z_{cp} were measured between the lower surface of the mobile magnet and the upper surface of the superconductor. As examples, see Figure 5 and Figure 6 that show the levitation and lateral force cycles measured on an MgB_2 cylinder with a NdFeB magnet, respectively.

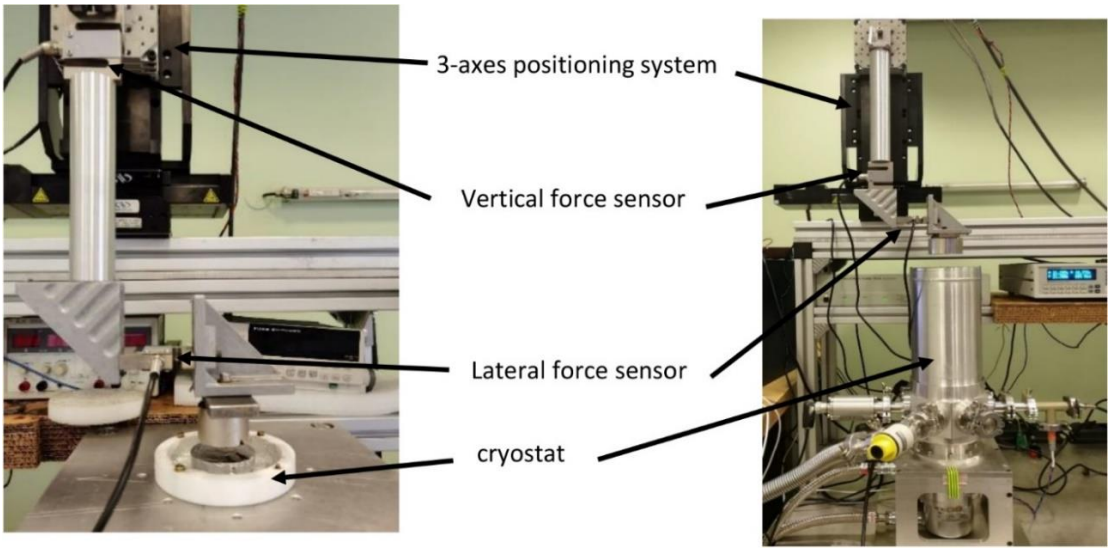

Figure 2 Cryostats and setups used for measuring the levitation and lateral forces at 77 K (left) and below 77 K (right).

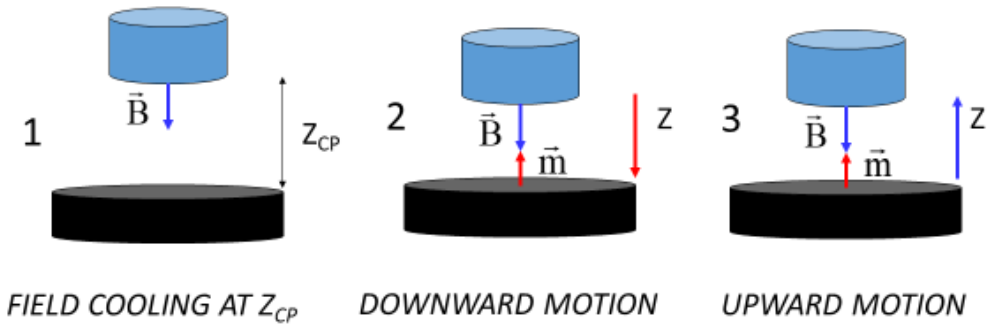

Figure 3 Process of measuring the levitation force: (1) superconductor(s) field cooling at a distance Z_{cp} from the mobile magnet, (2) downward motion of the mobile magnet to a distance Z_{min} from the superconductor, (3) upward motion of the magnet to Z_{cp} or above. In the figures, the superconductor is black, whereas the magnet is blue. The vector, $\vec{m}$, is the magnetization of the superconductor.

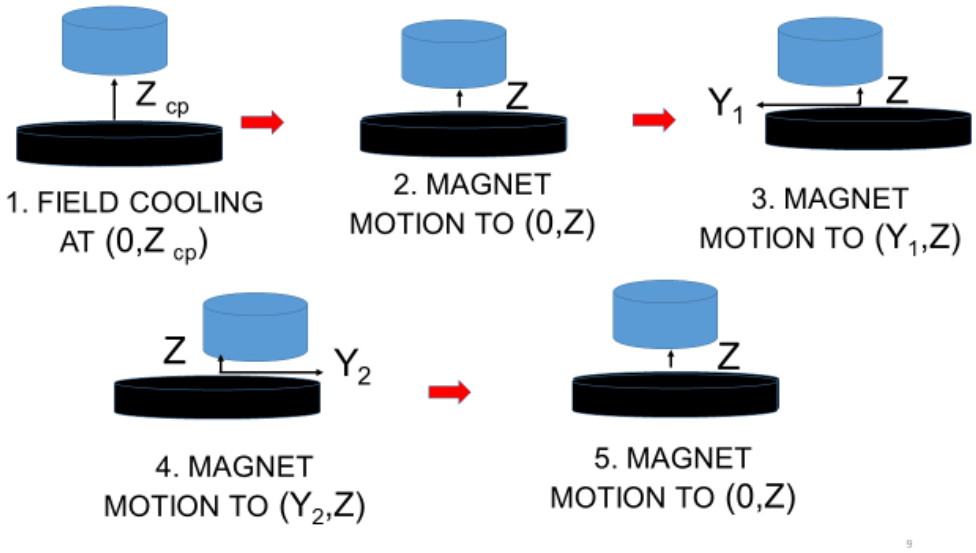

Figure 4 Process of measuring the lateral force: (1) superconductor field cooling at a distance Z_{cp} from the magnet, (2) vertical motion of the magnet to a distance Z from the superconductor, (3) lateral motion of the magnet to a distance Y_1, (4) lateral motion of the magnet to a distance Y_2, (5) magnet motion to (0,Z). In the figures, the magnet is blue, and the superconductor is black.

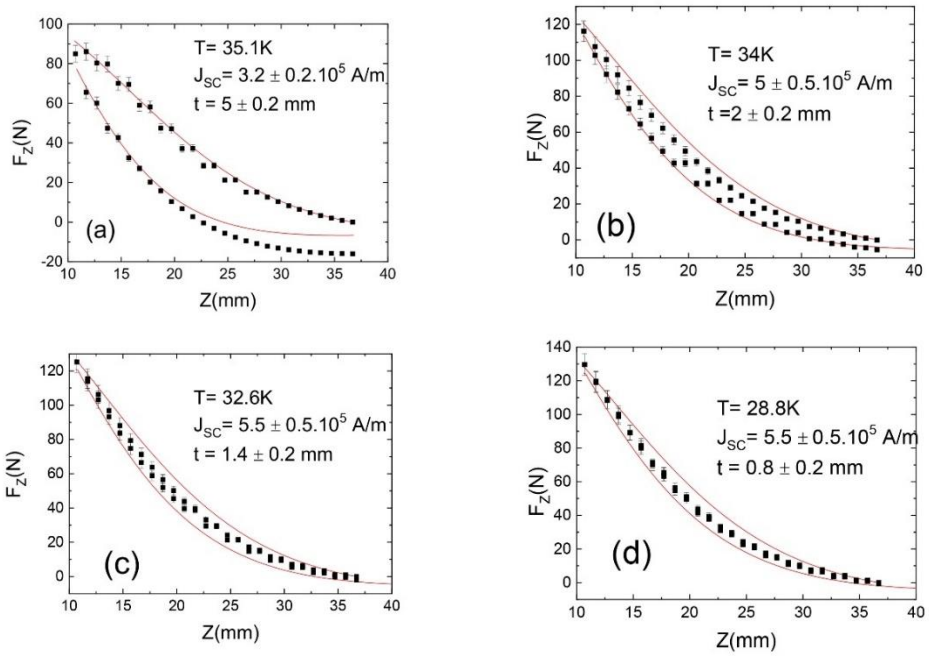

Figure 5 Levitation forces between an MgB_2 cylinder, with a diameter D = 59.6 mm and thickness h = 9.8 mm, and a 70 mm diameter and 30 mm thick NdFeB magnet at various temperatures. The superconductor was cooled down at a distance of Z_{cp} = 37 mm from the magnet. The filled squares represent the measured values. The upper (lower) continuous red line represents the results of the calculations reproducing these forces during the downward (upward) motion of the magnet with Eq. (8) (Eq. (13)).

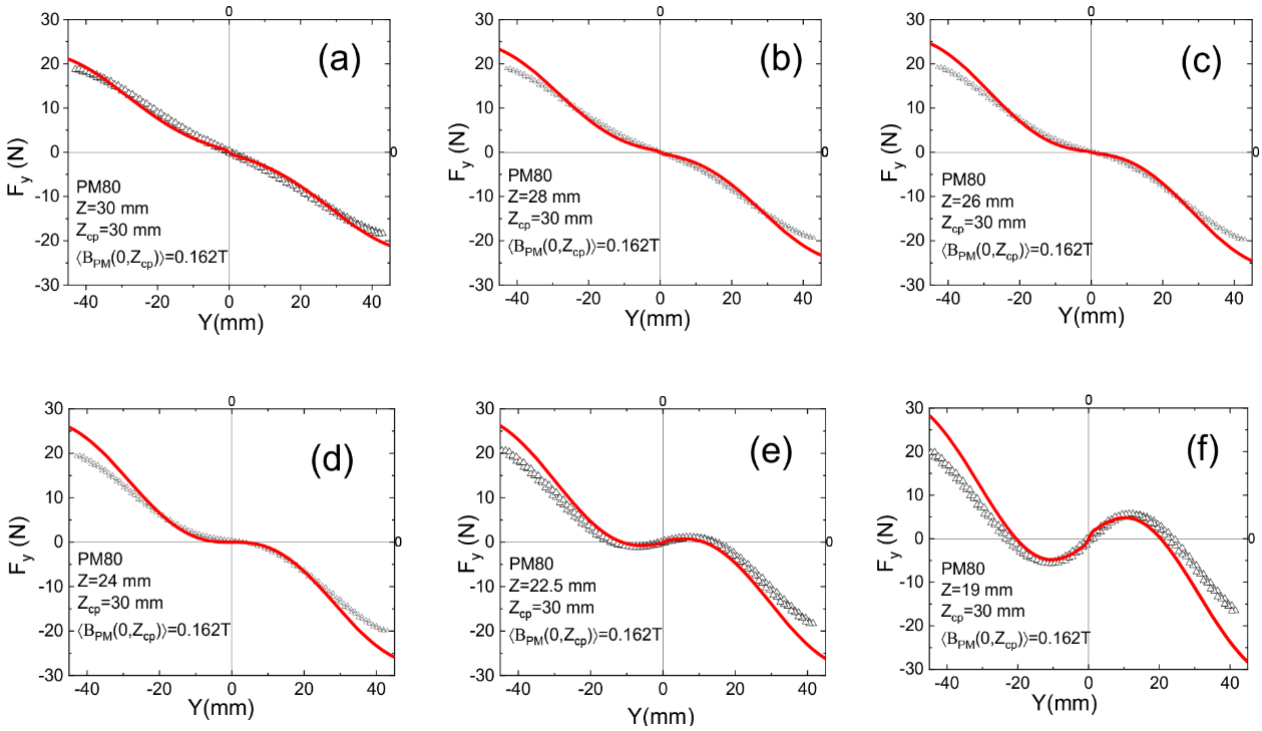

Figure 6 Lateral force, F_y, measured with the MgB_2 disc and the PM80 magnet at different magnet-superconductor separations after cooling down the MgB_2 disc at Z_{cp} = 30 mm. The open triangles denote the measurements, and the continuous red lines denote the radial forces, F_r, calculated with the model detailed in Section 3.3.

3. The Mean Field Model

In this section, we describe the physical bases of the model and then describe the calculations done for determining the levitation and the lateral forces as well as their domain of validity. As mentioned in the introduction, analytical models are practical in their use for simple superconductor shapes and regular distribution of the applied field. Hence, in the following, we consider only cylindrical superconductors and magnets with diameters D and D_{PM} and thicknesses h and $h_{PM,}$ respectively.

3.1 The Physical Bases of the Model

During the field cooling process, as long as the sample is in the normal state, the applied magnetic field penetrates the entire bulk. During the transition to the superconducting state at T_c, the magnetic flux is channeled along the vortex lines, and the field vanishes elsewhere in the superconductor. As detailed in [25], below T_c, for a constant applied field, the situation is frozen and no shielding current flows in the superconductor, the magnetic moment of which is equal to zero. Since the levitation force is due to the interaction of the shielding currents with the applied field, there is no levitation force at the cooling point (see Eq. (2)). As the relative positions of the magnet and of the superconductor change during the measurements, the field applied to the superconductor is modulated. We assume that due to the presence of barriers hindering the entry of vortices [26, 27], the modulation of the applied field results only in the generation of currents shielding the magnetic field variations and, as a result, of the magnetic moment, $\vec{m}$. As suggested

by Brandt [28], the magnetic images model [29, 30], and in our previous work [31], we write the force exerted on $\vec{m}$ by the external field $\vec{B}$ as

$$\vec{F} = \left[\vec{m} \cdot \vec{\nabla}\right]\vec{B}. \tag{3}$$

We now calculate the levitation and the lateral forces. The superconductors and the magnets have been taken as cylinders for the sake of simplicity and the cylindrical coordinates, *Z*, *r*, and ϑ, have been used for the calculations. The origin of the axes is along the symmetry axis of the superconductor at *Z* = 0. Otherwise, since the motion of the magnet during the measurement of the lateral force is radial along the *Y* axis, the lateral forces, F_r, calculated with the model must be compared to the measured F_y.

3.2 Calculation of the Levitation Force

Due to the symmetry of the system (see Figure 3), $\vec{m}$ is parallel to the disc axis, *Oz*, and we consider only the vertical component, m_z. Based on Eq. (3), we write the levitation force, F_z, as

$$F_z(Z) = m_z \frac{\partial B_z}{\partial Z} \tag{4}$$

where B_z is the vertical component of the magnet field along the axis of the sample. However, the field gradient generated by the magnet is nonuniform on the scale of the thickness of the bulk. Consequently, $\frac{\partial B_z}{\partial Z}$ is replaced in Eq. (4) by its value averaged on the thickness, *t*, of the part of the superconductor carrying the shielding currents:

$$\langle \frac{\partial B_z}{\partial Z} \rangle = \frac{1}{t} \int_t \frac{\partial B_z}{\partial Z} dZ \tag{5}$$

The magnetic moment, m_z, can be written according to the expression proposed by Brandt for the magnetic moment of a disk in an axial field [32]. Since the shielding currents are due to the modulation of the external field, here we consider that the field to be taken into account is the difference between the fields at the locations *Z* and Z_{cp}. These fields are nonuniform in the bulk, and in the framework of our mean-field approximations, we take their mean value calculated over the thickness *t*. As the magnet goes down, the resulting magnetic moment is

$$m_z = -\frac{2}{3} J_c t R^3 \left[cos^{-1}\left(\frac{1}{cosh\left(\frac{2\Delta B_a}{\mu_0 J_c t}\right)} \right) + \frac{sinh\left|\frac{2\Delta B_a}{\mu_0 J_c t}\right|}{cosh^2\left(\frac{2\Delta B_a}{\mu_0 J_c t}\right)} \right]. \tag{6}$$

where

$$\Delta B_a = \langle B_z(Z) \rangle - \langle B_z\left(Z_{cp}\right) \rangle \tag{7}$$

where $\langle B_z\left(Z_{cp}\right) \rangle$ and $\langle B_z(Z) \rangle$ are the values of the vertical components of the fields applied along the superconductor axis at the cooling point and at the distance *Z*, averaged over the thickness *t*. Finally, the levitation force during the downward motion of the magnet takes the form

$$F_z(Z) = m_z \langle \frac{\partial B_z}{\partial Z} \rangle \tag{8}$$

When the magnet motion is reversed at Z_{min}, the shielding currents present in the superconductor do not disappear. As a result, during the upward motion, the magnetic moment comprises two components

$$m_{max} = -\frac{2}{3} J_c t R^3 \left[cos^{-1} \left(\frac{1}{cosh\left(\frac{2\Delta B_{max}}{\mu_0 J_c t}\right)} \right) + \frac{sinh\left|\frac{2\Delta B_{max}}{\mu_0 J_c t}\right|}{cosh^2\left(\frac{2\Delta B_{max}}{\mu_0 J_c t}\right)} \right] \tag{9}$$

and

$$m_b = \frac{2}{3} J_c t R^3 \left[cos^{-1} \left(\frac{1}{cosh\left(\frac{2\Delta B_b}{\mu_0 J_c t}\right)} \right) + \frac{sinh\left|\frac{2\Delta B_b}{\mu_0 J_c t}\right|}{cosh^2\left(\frac{2\Delta B_b}{\mu_0 J_c t}\right)} \right] \tag{10}$$

where

$$\Delta B_{max} = \langle B_z(Z_{min}) \rangle - \langle B_z\left(Z_{cp}\right) \rangle \tag{11}$$

and

$$\Delta B_b = \langle B_z(Z) \rangle - \langle B_z(Z_{min}) \rangle. \tag{12}$$

The moment, $\vec{m}_{max}$, is generated by the currents that flow in the superconductor when the motion of the magnet is reversed. Currents resulting in the moment, $\vec{m}_b$, flow in the sample to compensate for the field variations between Z_{min} and Z. The currents creating the moments $\vec{m}_{max}$ and $\vec{m}_b$ flow in opposite directions, suggesting that they are located in different parts of the superconductors. While it is reasonable to suppose that the shielding currents flow in the part of the superconductor of thickness, t, that is facing the magnet during its downward motion, we have assumed that they flow in the areas shown in Figure 7 during the upward motion. As a consequence, F_z takes the form

$$F_z = m_{max} \left\langle \frac{\partial B_z(Z+t)}{\partial Z} \right\rangle + m_b \left\langle \frac{\partial B_z(Z)}{\partial Z} \right\rangle \tag{13}$$

for this part of the cycle. Otherwise, the measurements and calculations reported in [25, 33] result in $t \leq \frac{h}{2}$ for all the investigated samples and we have no insights on the current distribution for $t > \frac{h}{2}$. As a consequence, the model is valid for force cycles that can be reproduced with $t \leq \frac{h}{2}$ only. Since previous measurements have shown that t increases with increasing temperature [33], this constraint sets a high temperature limit for the model.

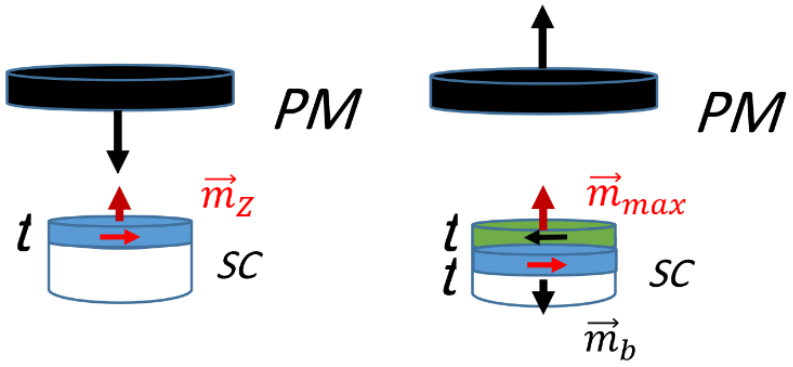

Figure 7 Assumed locations of the currents in the superconductor (SC) generating the moment $\vec{m}_Z$ during the downward motion of the magnet (PM) (left) and the moments $\vec{m}_b$ and $\vec{m}_{max}$ during the upward motion (right).

For the calculations, since the surface current density of the sample $J_{SC} = J_c t$ is present in Eqs. (6), (9), and (10), we take this quantity and the thickness, *t*, as the fitting parameters to reproduce the measurements with Eqs. (8) and (13). Consequently, the fitting process gives J_{SC}, *t*, and J_c. Figure **5** shows the levitation forces between an MgB_2 cylinder, with a diameter *D* = 59.6 mm and thickness *h* = 9.8 mm, and a 70 mm diameter and 30 mm thick NdFeB magnet measured at various temperatures. The superconductor was cooled down at a distance of Z_{cp} = 37 mm from the magnet. The continuous red lines show the results of the calculations carried out with Eqs. (8) and (13) taking, for J_{sc} and *t*, the values indicated in each graph shown in Figure 5. The surface critical current density increases from 35.1 K (Figure 6(a)) to 34 K (Figure 6(b)) and is almost constant at lower temperatures (Figures 6(c) and 6(d)), similar to the trend exhibited by the levitation force. As expected, the thickness *t* is an increasing function of the temperature.

3.3 Calculation of the Lateral Force and Determination of the Stability of the Levitating System

We consider only the superconducting cylinders with $D \gg h$. Consequently, a possible radial component of $\vec{m}$ is much smaller than the vertical one, and we do not take it into account. Otherwise, we take the sign of $\frac{\partial F_r}{\partial r}$ near *r* = 0 as an indicator of stability. This quantity is positive for two magnets with opposite magnetization and negative if the levitation is stable. Using Eq. (3), we have

$$F_r = m_z \frac{\partial B_r}{\partial Z} \tag{14}$$

Since the magnetic field is generated by an external source, we have

$$\vec{\nabla} \times \vec{B} = 0 \quad \text{and} \quad \frac{\partial B_r}{\partial Z} = \frac{\partial B_Z}{\partial r} \tag{15}$$

and F_r can be written as

$$F_r = m_z \frac{\partial B_Z}{\partial r}. \tag{16}$$

The magnetic moment, m_z, takes the same form as in Eq. (6). However, since the system is not axisymmetric for r ≠ 0, we assume that

$$\Delta B_a = \langle B\left(0, Z_{cp}\right)\rangle - B_\phi(r, Z) \tag{17}$$

where

$$B_\phi(r, Z) = \frac{\phi(r, Z)}{\pi \frac{D_{sc}^2}{4}}. \tag{18}$$

where $\phi(r, Z)$ is the flux of the mean value on the thickness, t, of the field threading the disc when the magnet is at the location (r, Z). There are various techniques permitting one to calculate this quantity. As an example, in Appendix I, we describe the technique we have used for reproducing the measurements reported in Figure 6 and Figure 8. Otherwise, the modulation of r results in that of $B_\phi(r, Z)$ only. Consequently, F_r can be written as

$$F_r = m_Z \frac{\partial B_\phi(r, Z)}{\partial r} \tag{19}$$

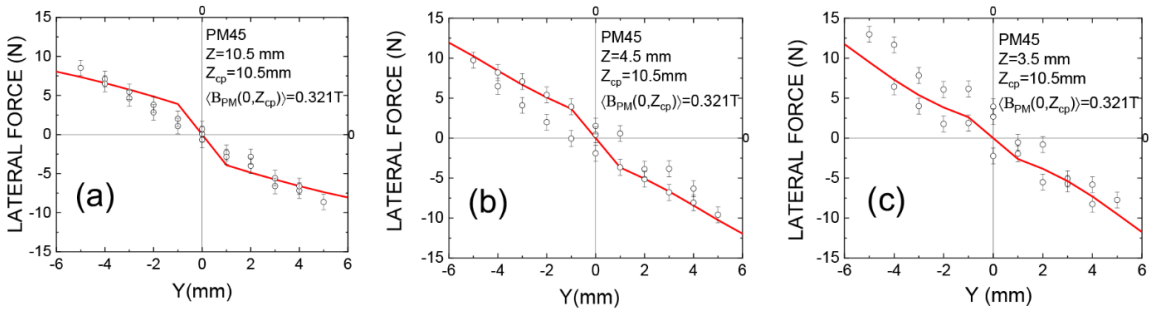

Figure 8 Lateral force, F_y, measured with the YBCO disc and the PM45 magnet at various magnet-superconductor distances after cooling down the disc at Z_{cp} = 10.5 mm. The open circles denote the measurements, and the continuous red lines denote the radial forces, F_r, calculated with the model detailed in Section 3.3.

An important consequence of Eqs. (16) to (19) is that, depending on the relative values of $\langle B\left(0, Z_{cp}\right)\rangle$ and $B_\phi(r, Z)$, m_Z and $\frac{\partial F_r}{\partial r}$ are either positive or negative and the levitating system is either stable or unstable. We emphasize that since we have not considered the changes in the shielding currents resulting from the reversal of the magnet motion, the model does not account for a possible hysteresis of the lateral force.

As examples, we report the measurements carried out using cylindrical NdFeB magnets and superconductors, the dimensions of which are given in Table 1. Figure 6 and Figure 8 present the values of $F_Y(Y)$ at different Z, plotted as open symbols, after (i) cooling down the MgB_2 cylinder at 20 K at a distance of Z_{cp} = 30 mm from the PM80 magnet and (ii) cooling down the $YBa_2Cu_3O_{7-\delta}$ (YCBO) cylinder at 77 K at a distance of Z_{cp} = 10.5 mm from the PM45 magnet. The continuous red lines show the $F_r(r)$ resulting from the calculations done using Eqs. (16) to (19) by taking the values obtained for J_{SC} and t from the calculations of F_Z, which are reported in Table 2.

Table 1 Diameters (D), and thicknesses (h) of the cylindrical superconductors and magnets used for the reported measurements.

SUPERCONDUCTING CYLINDERS		
Material	D (mm)	h (mm)
MgB_2	70	30
YBCO	56	10
NdFeB PERMANENT MAGNETS		
PM45	45	30
PM80	80	30

Table 2 Values of the surface critical current density, J_{SC}, and the thickness, t, resulting from the calculation of F_Z and used for reproducing the lateral forces of the MgB_2 and the YBCO samples shown in Figure 7 and Figure 8, respectively.

	J_{SC} (A/m)	t (mm)
MgB_2	~2.10^5	~0.2
YBCO	~$2.6.10^6$	~3.2

In the case of the measurements carried out with the MgB_2 disc, the calculated forces increasingly deviate from the measurements as $\Delta Z = Z_{cp} - Z$ increases for large Y values. However, the lateral force is satisfactorily reproduced in the vicinity of $Y = 0$, i.e., the area of interest. The slopes of the $F_y(Y)$ graphs near $Y = 0$ show that the lateral force stabilizes the magnet above the superconductor if $Z \geq 24$ mm and that levitation is unstable for Z < 24 mm. Otherwise, the levitation of the YBCO cylinder is stable at least down to 3.5 mm. We emphasize here that the model accounts for the transition from the stable to the unstable regime with good accuracy. Stability exists only if

$$B_\phi(0, Z) \leq \langle B\left(0, Z_{cp}\right)\rangle \tag{20}$$

This can be verified by comparing Figures 7 and Figure 8 to Figure 9, which shows $B_\phi(r, Z)$ and $\langle B\left(0, Z_{cp}\right)\rangle$ for both discs. The lateral force at Z_{cp} is always a stabilizing force because $\langle B\left(0, Z_{cp}\right)\rangle$ is the largest field applied to the layer of the superconductor carrying the currents at the cooling point. As Z decreases, the field generated by the permanent magnet increases, as does $B_\phi(r, Z)$ in the vicinity of $r = 0$, and instability occurs if Eq. (20) is no longer verified. This does not happen with the system comprising the YBCO disc because the superconductor diameter is larger than that of the magnet. As a result, the difference between $\langle B\left(0, Z_{cp}\right)\rangle$ and $B_\phi\left(0, Z_{cp}\right)$ is much larger than in the system consisting of the MgB_2 disc and the PM80 magnet.

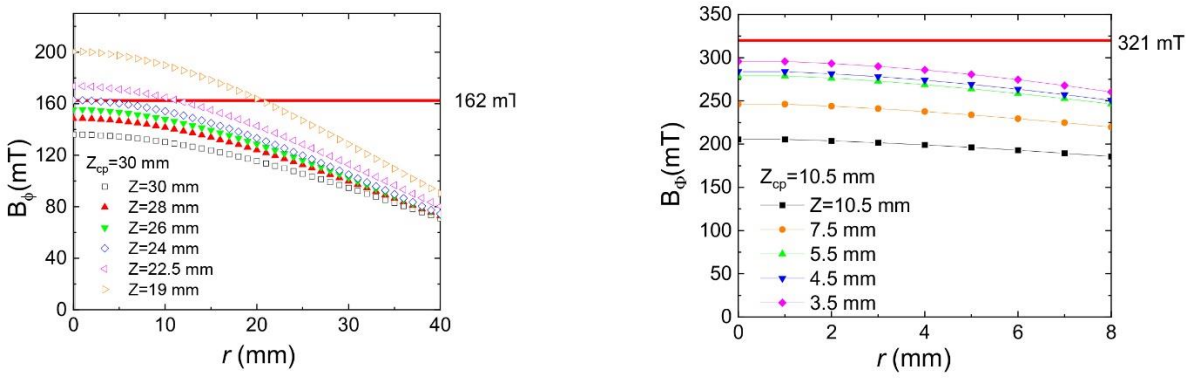

Figure 9 Mean value, B_Φ, of the field applied by (i) the magnet PM80 to the MgB_2 disc (left) and (ii) the magnet PM45 to the YBCO disc (right), as a function of the position, *r*, of the axis of the disc with respect to the magnet axis. The horizontal red lines denote $\langle B(0, Z_{cp})\rangle$.

4. Advantages and Limitations of the Model

The validity of the model is supported by the modulation of the thickness, *t*, of the layers carrying the shielding currents as the temperature decreases. Numerical simulations suppose, as a general rule, that the currents flow in the entire sample irrespective of the temperature [15-19]. This hypothesis is inconsistent with the suggestion that as the temperature decreases, the behavior of the superconductor tends toward the Meissner limit, a situation in which the current flows on the superconductor surface facing the permanent magnet only [34]. In contrast, calculations performed using the mean-field model result in decreasing values of *t* as the temperature decreases [25, 33], i.e., coming nearer to the Meissner limit. Otherwise, applying the mean-field model requires only measuring or calculating the vertical component of the magnetic field along the magnet axis for determining the levitation forces and along the magnet radius at different Z for calculating the lateral ones (see Appendix I). This is in contrast to the numerical simulations that require knowledge of the field components in the entire superconductor and the surrounding region. This contributes to reducing the time required for performing the calculations. However, there are limitations in using the model, which are set in the first place by the requirement to have superconductors and magnets with a high degree of symmetry. In addition, the temperature must be low enough to result in $t \leq \frac{h}{2}$. Finally, the model supposes that the vortex density does not change with the applied field, which would not be the case if either the applied field was larger than the vortex penetration field of the superconductor or if flux jumps occurred, as this has been observed at low temperatures [35]. We also mention here that for low $\frac{2\Delta B_a}{\mu_0 J_{SC}}$ ratios, which are generally encountered at low temperatures and for which J_c and J_{SC} are large, the magnetic moments m_z, m_{max}, and m_b tend toward saturation. As a result, good reproduction of the measured levitation force can be obtained with a large range of J_{SC} values, which makes the accurate determination of this quantity difficult. This is the case for the values reported in Table 2. Conversely, for designing a cylindrical levitation system, the maximum levitation force can be evaluated using Eqs. (5) to (8) by taking an arbitrarily large value for J_{sc} and varying *t* between 0 and *t*/2. The range of working heights in which levitation

is stable can be *a priori* determined as a function of the selected cooling height from the knowledge of the field generated by the magnet using Eq. (20).

5. Conclusions

In this study, we have described an analytical mean-field model that reproduces the levitation and lateral forces applied to superconductors in levitating systems consisting of cylindrical magnets and superconductors. We have stated its domain of validity and verified that the measurements carried out with levitating MgB_2 and YBCO superconductors are in agreement with the calculated values. One of the advantages of the described technique is to give an estimation of (i) the surface critical current, J_{SC}, and (ii) the thickness, t, of the layer carrying the shielding currents. However, the most important result of this work is that, in order to be stable, axisymmetric levitating systems must work in conditions in which Eq. (20) is valid.

Author Contributions

Pr Jacques Noudem: Project development. Dr Yteng Xing: Experimental set-ups and measurements. Pr Pierre Bernstein: modeling.

Competing Interests

The authors have declared that no competing interests exist.

Additional Materials

The following additional materials are uploaded at the page of this paper.

1. Appendix I.

References

1. Lin QX, Wang WJ, Deng ZG, Jiang DH, Shin DI, Xie ZG, et al. Measurement and calculation method of the radial stiffness of radial high-temperature superconducting bearings. J Supercond Nov Magn. 2015; 28: 1681-1685.
2. Morandi A, Perini E, Giunchi G, Fabbri M. Numerical analysis and experimental measurements of magnetic bearings based on MgB_2 hollow cylinders. IEEE Trans Appl Supercond. 2010; 21: 1460-1463.
3. Walter H, Bock J, Frohne C, Schippl K, May H, Canders WR, et al. First heavy load bearing for industrial application with shaft loads up to 10 kN. J Phys Conf Ser. 2006; 43: 995.
4. Werfel FN, Floegel-Delor U, Rothfeld R, Riedel T, Goebel B, Wippich D, et al. Superconductor bearings, flywheels and transportation. Supercond Sci Technol. 2011; 25: 014007.
5. Wang J, Wang S, Zeng Y, Huang H, Luo F, Xu Z, et al. The first man-loading high temperature superconducting Maglev test vehicle in the world. Physica C Supercond. 2002; 378: 809-814.
6. Sotelo GG, Dias DH, Machado OJ, David ED, de Andrade Jr R, Stephan RM, et al. Experiments in a real scale maglev vehicle prototype. J Phys Conf Ser. 2010; 234: 032054.

7. Sotelo GG, Dias DH, Motta ES, Sass F, Ferreira AC, de Andrade Jr R, et al. Operational tests of a full scale superconducting MagLevehicle Unit. Phys Procedia. 2012; 36: 943-947.
8. Wang JS, Wang SY, Deng CY, Zeng YW, Song HH, Zheng J, et al. Design consideration of a high temperature superconductor Maglev vehicle system. IEEE Trans Appl Supercond. 2005; 15: 2273-2276.
9. Deng Z, Zhang W, Zheng J, Ren Y, Jiang D, Zheng X, et al. A high-temperature superconducting maglev ring test line developed in Chengdu, China. IEEE Trans Appl Supercond. 2016; 26: 3602408.
10. Zheng B, Zheng J, He D, Ren Y, Deng Z. Magnetic characteristics of permanent magnet guideways at low temperature and its effect on the levitation force of bulk YBaCuO superconductors. J Alloys Compd. 2016; 656: 77-81.
11. Mattos LS, Rodriguez E, Costa F, Sotelo GG, De Andrade R, Stephan RM. MagLev-Cobra operational tests. IEEE Trans Appl Supercond. 2016; 26: 3600704.
12. CCTV+. China unveils prototype superfast maglev train [Internet]. Beijing: CCTV+; 2021. Available from: https://www.cctvplus.com/news/20210113/8173467.shtml#!language=1.
13. Wang J, Wang S, Deng C, Zheng J, Song H, He Q, et al. Laboratory-scale high temperature superconducting Maglev launch system. IEEE Trans Appl Supercond. 2007; 17: 2091-2094.
14. Zheng X, Yang Y. Transition cooling height of high-temperature superconductor levitation system. IEEE Trans Appl Supercond. 2007; 17: 3862-3866.
15. Quéval L, Liu K, Yang W, Zermeño VM, Ma G. Superconducting magnetic bearings simulation using an H-formulation finite element model. Supercond Sci Technol. 2018; 31: 084001.
16. Sass F, Sotelo GG, de Andrade Junior R, Sirois F. H-formulation for simulating levitation forces acting on HTS bulks and stacks of 2G coated conductors. Supercond Sci Technol. 2015; 28: 125012.
17. Ma GT. Considerations on the finite-element simulation of high-temperature superconductors for magnetic levitation purposes. IEEE Trans Appl Supercond. 2013; 23: 3601609.
18. Ma GT, Ye CQ, Liu K, Mei GM, Zhang H, Li XT. Geometrical effects on the levitation capability of multiseeded Y–Ba–Cu–O blocks. IEEE Trans Appl Supercond. 2015; 26: 3600205.
19. Sass F, Dias DH, Sotelo GG, de Andrade Junior R. Superconducting magnetic bearings with bulks and 2G HTS stacks: Comparison between simulations using H and AV formulations with measurements. Supercond Sci Technol. 2018; 31: 025006.
20. Kordyuk AA. Magnetic levitation for hard superconductors. J Appl Phys. 1998; 83: 610-612.
21. Hull JR, Cansiz A. Vertical and lateral forces between a permanent magnet and a high-temperature superconductor. J Appl Phys. 1999; 86: 6396-6404.
22. Zhang M, Han Y, Guo X, Zhao C, Deng F. The connection characteristics of flux pinned docking interface. J Appl Phys. 2017; 121: 113907.
23. Yang W, Liao D, Ji Y, Yao L. Effects of magnetization conditions on dynamic characteristics of spacecrafts with superconducting flux pinning docking interfaces. J Appl Phys. 2018; 124: 213901.
24. Qin MJ, Li G, Liu HK, Dou SX, Brandt EH. Calculation of the hysteretic force between a superconductor and a magnet. Phys Rev B. 2002; 66: 024516.
25. Bernstein P, Noudem J, Dupont L. Critical current density and current distribution in field cooled superconducting disks. Supercond Sci Technol. 2016; 29: 075007.
26. Bean CP, Livingston JD. Surface barrier in type-II superconductors. Phys Rev Lett. 1964; 12: 14.

27. Hernández AD, Dominguez D. Surface barrier in mesoscopic type-I and type-II superconductors. Phys Rev B. 2002; 65: 144529.
28. Brandt EH. Levitation in physics. Science. 1989; 243: 349-355.
29. Yang Y, Zheng X. Method for solution of the interaction between superconductor and permanent magnet. J Appl Phys. 2007; 101: 113922.
30. Xu KX, Cao Y, Hu SB, Zuo PX, Li GD. Modeling of hysteretic behavior of the levitation force between superconductor and permanent magnet. Physica C Supercond. 2013; 486: 17-22.
31. Xing Y, Bernstein P, Noudem J. Superconductor-magnetic levitation: Investigation of the restoring force. IEEE Trans Appl Supercond. 2021; 31: 1-4.
32. Brandt EH. Superconductor disks and cylinders in an axial magnetic field. I. Flux penetration and magnetization curves. Phys Rev B. 1998; 58: 6506.
33. Bernstein P, Colson L, Dupont L, Noudem J. A new approach to the current distribution in field cooled superconductors disks. Supercond Sci Technol. 2017; 31: 015008.
34. Badıa A, Freyhardt HC. Meissner state properties of a superconducting disk in a non-uniform magnetic field. J Appl Phys. 1998; 83: 2681-2688.
35. Korotkov VS, Krasnoperov EP, Kartamyshev AA. Flux jumps at pulsed field magnetization. J Supercond Nov Magn. 2016; 29: 1893-1896.